Pre-Registered Structural Predictions for LHC Run-3 Dijet Angular Distributions from a Discrete Emergent Universe Model

Jason Merwin
Independent researcher

July 2026

Abstract

We present pre-registered, cryptographically frozen structural predictions for CMS Run-3 dijet angular distributions $(1/\sigma)\, d\sigma/d\chi$ at 13.6 TeV, derived from the Discrete Emergent Universe (DEU) computational framework. Under a single published energy anchor ($E24 \leftrightarrow 6.14$ TeV) and a two-stage pre-registration protocol frozen before any profiling simulation existed, the model predicts: a pre-boundary excess accumulating at $1 < \chi < 2$ with a soft-wall deficit immediately above $\chi = 2$ in the 7–8 TeV dijet mass bin; and, above 8 TeV, an inversion of the post-boundary deficit to a weak excess as the boundary softens and leaks, with the negative step S^* and edge-log-drop Δ^* persisting in both bins. All prediction values trace through SHA-256 hashes to simulation instruments certified row-exact against the archived output of the original DEU collision campaign. We additionally report the profiling ladder beyond the scored range, which exhibits a previously uncharacterized regime of simultaneous channel extinction, and an exploratory analysis of collision phenomenology versus foam age whose central qualitative claims are shown to be robust across a declared band of instrument-reconstruction uncertainties. Negative results obtained during the campaign—including a refuted selection-artifact hypothesis and an underived component-selection convention that quarantined one full simulation run—are documented with the same prominence as positive findings.

1 Introduction

In the Standard Model, the physical vacuum is treated as a continuous, infinite stage where high-energy particles scatter in seamless, unbroken curves. Searches for Beyond Standard Model (BSM) physics—such as quark compositeness or novel contact interactions—typically parameterize deviations as smooth, continuous enhancements at low χ [8, 9]. In contrast, the Discrete Emergent Universe (DEU) framework defines spacetime as a relational network emerging from the fundamental combinatorics of distinction ($A \neq B$). As these structures expand, they produce a combinatorial "foam" in which particles are recognized not as point masses, but as persistent topological defects, and where geometry and forces emerge purely from the local routing of information [3, 4, 10].

Previous work demonstrated that these topological defects could be driven together to mimic high-energy particle collisions, yielding debris patterns strikingly similar to those observed at the LHC [2]. Specifically, these simulated collisions predicted a distinct, non-Standard Model anomaly in CMS particle-level dijet distributions at 13 TeV. This anomaly manifested as a macroscopic lattice fracture: a 30.5% residual cross-section excess piling up immediately prior to the $\chi = 2$ boundary, followed by an abrupt post-boundary collapse in the 6.0 to 7.0 TeV mass bin. While this residual "stutter" structure was ultimately confirmed in actual dijet spectra, our theoretical prediction reached completion approximately one month after the corresponding experimental observation was published [1, 2]. Despite the striking success of the DEU model to predict the observed phenomena, the timing of the publications rendered the evidential value to retro-diction.

The present campaign was rigorously designed to publicly lock DEU predictions at higher energy collisions prior to their publication. To guarantee strict predictive integrity, every observable, binning choice, statistic, classification threshold, and scoring rule was cryptographically frozen and hashed (Stage 1, tag `run3-protocol-v1`) before any profiling simulation was generated. Furthermore, the numerical prediction values themselves were frozen and hashed (Stage 2, tag `run3-values-v1`, the subject of this document) well in advance of any relevant LHC Run-3 data publication. Within this transparent framework, any procedural deviations are reported as protocol violations rather than being edited away, and underpowered or null outcomes are treated as permanent, publicly documented results.

2 Framework and Energy Dictionary

The DEU models the vacuum as a discrete activation foam evolved by a deterministic engine (K3, v0.4)[6]; high-energy collisions correspond to driven contact cascades ("funnels") between zero-anchor frontier structures, followed by fracture into debris[2]. Graph tiers map to dijet invariant mass through the single published anchor $E24 \leftrightarrow 6.14$ TeV, giving $m_{jj}(E) = 0.2558333\,E$ TeV (protocol §1.1). No center-of-mass mapping is claimed or used. The claim scope is structural: boundary steps, cliff/leakage patterns, and their tier trend in publication-format observables—not cross-sections, event-level sprays, or detector quantities (§1.3).

3 Pre-Registration Protocol

Stage 1 froze: the observable family (χ distributions with the shared bin edge at $\chi = 2$, mass bins [5–6], [6–7], [7–8], >8 TeV); the four predicted quantities per bin (sign and magnitude class of the pre-boundary residual R_L, post-boundary residual R_R, step $S^* = R_R - R_L$, and edge-log-drop Δ^*); magnitude-class edges (null $< 0.05 \leq$ weak $< 0.15 \leq$ strong $< 0.35 \leq$ extreme); the regime-discrimination statistics; the simulation protocol including an ordered-reserve seed policy; a structurally firewalled eligibility function with no code path to outcome data; and an outcome-blind classifier with frozen thresholds. Scoring (§10): directional hits on signs of S^* and Δ^* per bin, Stouffer-aggregated, with pre-declared falsifiers including sign failure in at least half of scored bins and boundary structure appearing at $\chi \neq 2$ with the predicted signature while $\chi = 2$ shows none.

4 Instruments and Provenance

The original campaign's instruments predate this work; the scaffold reconstructs them under an exactness rule (§2.2 of the protocol): a reconstructed instrument is valid only upon exact reproduction of archived reference outputs. The route-funnel replayer and fracture stage are certified row-exact and byte-identical, respectively, against the archived $E30$ ledgers. The scan's generative core is certified exact against the archived $E30$ payload, with a declared open gap: the original component-candidate filter is underived—no predicate over certified-scope component properties reproduces the archived membership (§9)—which blocks certified scans on substrates other than the archived state.

Consequently, all scored predictions are computed in **archived scope**: candidate components and bank pairs are taken directly from the original instrument's archived output at the archived state (round 1,910,001), and families are produced by the certified exact-capacity enumeration over that bank. No reconstructed candidate selection touches any scored number. The drive pipeline operating on these families was re-certified in situ: driving the archived $E30$ family from the working snapshot reproduces the certified funnel ledger row-exact, including every bridge χ value, and reproduces the anchor statistics (15/15 contacts at rank 0, peak, χ median 1.890).

Simulation-to-observable mapping. (Stage 2, frozen with the values.) The per-contact bridge χ population of the primary (top-bank, protocol §5.4) drive is read as the predicted excess structure relative to a smooth continuum. The choice of the bridge population over fracture-debris capsules was ratified before hashing on grounds independent of the resulting values: the dictionary's anchor statistic (χ median 1.890 at $E30$) is a bridge quantity; the pre-existing $E30$ "soft wall" designation is reproduced by the bridge population under the frozen thresholds; and the debris population is wall-empty even on the certified anchor. The full mapping (m1–m9) is embedded verbatim in the frozen prediction card.

5 Locked Predictions

Mass bin	R_L	R_R	S^*	Δ^*	Boundary structure
$[5, 6]$ TeV	VOID (no populated tier in scored range)				
$[6, 7]$ TeV	VOID; $E24$ control: $p_L = 0.667$, $p_R = 0.083$, soft-wall				
$[7, 8]$ TeV	+ extreme	− extreme	− extreme	− strong	soft-wall
>8 TeV	+ extreme	+ weak	− extreme	− strong	populated

Table 1: Frozen Stage-2 prediction card (tag `run3-values-v1`). Pooled statistics: $[7, 8]$ TeV (tiers $E28$, $E30$; 29 contacts) $p_L = 0.655$, $p_R = 0.069$; >8 TeV (tiers $E32$–$E36$; 51 contacts) $p_L = 0.529$, $p_R = 0.098$. Ordinal trend (§3.3): soft-wall → populated.

In physical terms: rather than a smooth continuum or a classic resonance peak, the model predicts a macroscopic structural artifact. We anticipate an excess piling up just below $\chi = 2$ with a suppressed step across it at 7–8 TeV. Above 8 TeV, this boundary does not sharpen into a new BSM particle resonance; instead, the wall softens and leaks—the post-boundary deficit inverts to a weak excess while the step and edge-drop persist. The R_R sign inversion between bins is the highest-risk single element of the card. Because continuum models cannot naturally produce discrete geometric step-drops that soften with energy, this provides a rigid, parameter-free structural falsifier entirely distinct from standard effective field theory expectations. The unscored $E24$ bracketing control (6.14 TeV, the dictionary's anchor point) lands in the same structural class as the adjacent scored bin.

6 Simulation Results in the Scored Range

Across prediction tiers $E24$–$E36$ on the mature archived substrate, the top-bank two-frontier drive reaches strict peak at every tier (P(2f max-cap) = 1.0, funnel linearity deviation 0 throughout), with the bridge χ median rising monotonically through the anchor value and crossing the $\chi = 2$ boundary precisely at $E36$: 1.404, 1.328, 1.891, 1.689, 1.891, 2.002 for $E24$–$E36$, with the above-boundary fraction rising 0.33 → 0.50.

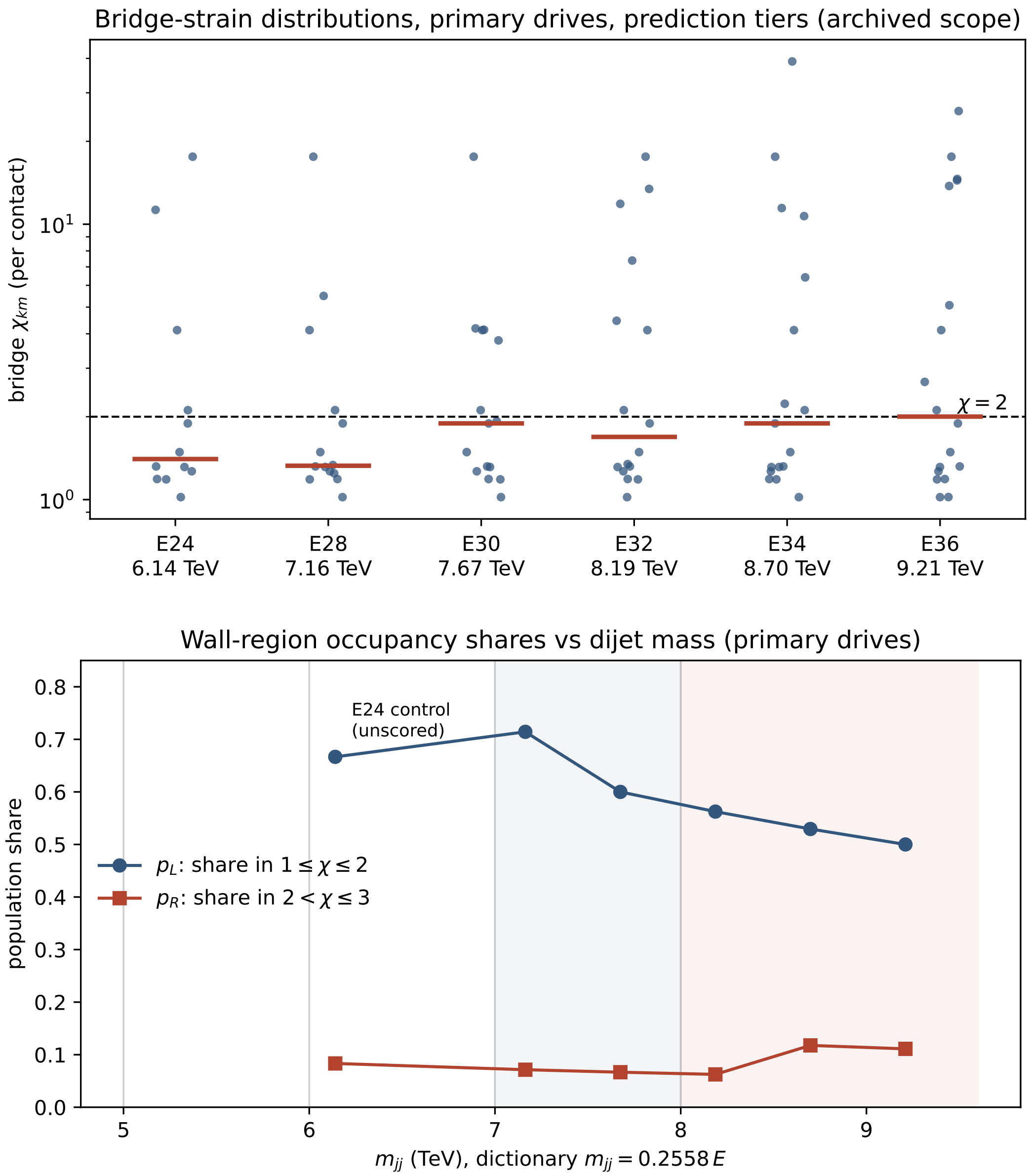

Figure 1: Top: bridge-strain distributions of the primary drives across prediction tiers; medians in red, the $\chi = 2$ boundary dashed. Bottom: wall-region occupancy shares versus dijet mass; scored bins shaded.

7 Profiling Beyond the Scored Range: Simultaneous Extinction

The profiling ladder ($E36$–$E54$, same certified scope) reveals a regime transition not anticipated by the frozen §4.5 dichotomy of monotone softening versus channel fragmentation, and reported per its mixed clause. Two-frontier family availability under archived scope collapses monotonically—290, 82, 30, 15, 13, 7, 2, 0, 0, 0 for $E24$ through $E54$—with two-frontier channels extinct at $E48$ and above, where collisions can only route through composite decompositions. Simultaneously, peak capability fails: above $E36$ every drive of every class stalls exactly one contact short of peak on its trailing frontier. The $\chi = 2$ wall region, richly populated at $E30$, evacuates with rising tier. We term this *simultaneous extinction*: concentrated channels vanish and completion fails together, the mechanism underlying the predicted softening of boundary structure with mass.

Terminal spectrum. The extinction regime terminates in discrete structure. Under the certified ($\leq$3-frontier) enumeration over the archived bank, family availability ends not with a fade but with a forbidden gap and an isolated terminal line: 9 families at $E56$, 3 at $E58$, none at $E60$ ($m_{jj} \approx$ 15.35 TeV, arithmetically unreachable — no disjoint capacity combination sums to $N_0 = 30$), and exactly one at $E62$ ($\approx$ 15.86 TeV): the 11+10+10 family assembled from the bank's three strongest pairs, $N_0 = 31$ being the maximum attainable capacity sum. Driven, this terminal channel locks 30 of 31 contacts at rank 0 and stalls one short on its trailing frontier — the one-short signature of the extinction regime holding at the last allowed energy; its bridge sequence opens with the eleven strains of the $E30$ anchor itself, the shared dominant pair linking the dictionary's calibration point to the vacuum's terminal collision. Both the gap and the line are stated relative to the certified instrument's family scope and the archived substrate; higher-multiplicity routing and substrate dependence are open questions. A forbidden energy level below an isolated terminal line is, to our knowledge, a signature only a discrete capacity spectrum produces, and we record it as the model's own statement of its extreme regime.

8 Epoch Dependence of Collision Phenomenology (Exploratory)

If the DEU's foam is modeling expanding universe, its collision phenomenology should depend on cosmic age. An exploratory single-seed sweep ($E30$ capacity, ages 2.5×10^5–8×10^6 engine rounds) exhibits an epochal arc; because these sweeps use the reconstruction's unfiltered candidate scope (§9), every claim below was re-derived under a declared six-member band of candidate filters spanning the reconstruction uncertainty.

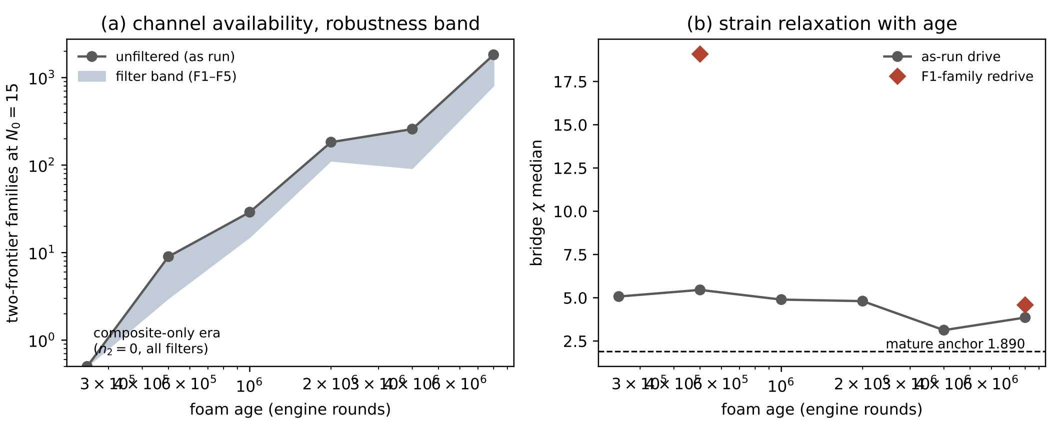

Figure 2: Top: bridge-strain distributions of the primary drives across prediction tiers; medians in red, the $\chi = 2$ boundary dashed. Bottom: wall-region occupancy shares versus dijet mass; scored bins shaded.

We emphasize that "cosmic age" in this context refers strictly to the topological maturity of the computational substrate—the progressive accumulation of combinatorial capacity and stable routing channels. Engine rounds represent the iterative ticks of the model's bandwidth scheduler, not a global physical clock. Consequently, no linear calibration is claimed between the DEU engine rounds observed here and specific physical cosmological epochs (e.g., the quark or hadron epochs) measured in seconds since the Big Bang. The observed arc demonstrates that modern collision phenomenology requires a mature, complex substrate to support concentrated channels, but mapping this topological maturation to the standard cosmological timeline remains outside the scope of this structural prediction.

Robust under the entire band: a primordial composite-only era—at 2.5×10^5 rounds no two-frontier family exists under any filter while composite families do—and the emergence of two-frontier channels by 5×10^5 rounds under every filter. **Robust in aggregate:** growth of channel availability by three orders of magnitude from emergence to 8×10^6 rounds; however, strict monotonicity is filter-sensitive (a 2M $\rightarrow$ 4M dip appears under edge-thresholded filters), and absolute counts carry a factor $\approx$2 instrument uncertainty (filtered counts are 50–70% of baseline).

Selection sensitivity. Family selection is filter-invariant at ages 1M–4M. At the two filter-sensitive ages, re-drives under the strictest near-miss filter's alternate top family show: peak status and perfect funnel linearity reproduce at both ages (selection-robust); χ magnitude is family-stable in the late epoch (8×10^6 rounds: median 4.58 versus 3.857 as run, both far above the mature anchor's 1.890) and strongly family-sensitive at emergence (5×10^5 rounds: median 19.1 versus 5.455 as run). Early-epoch strain is therefore reported at regime level—strongly elevated, family-dependent—rather than as point values. The claims that young-foam drives reach peak and that χ does not relax to the mature anchor within 8×10^6 rounds are robust under both family choices.

The arc bookends the tier structure of §7: composite-only regimes appear at both extremes—the young universe, where concentrated channels have not yet formed, and the high-energy frontier, where they have gone extinct. Collision phenomenology matures with cosmic age toward the two-frontier-supported modern epoch and de-matures with collision energy; the archived mature substrate used for all scored predictions sits in the modern epoch by construction and by continuity with the published anchor.

9 Negative Results and Instrument Limitations

Reported per program practice at equal prominence.

9.1 Selection-artifact hypothesis, refuted. The elevated strain in fresh-foam cohorts was hypothesized to stem from a family-selection divergence between orchestrators and the original instrument. A pre-registered proxy over certified geometry columns failed validation (0/7 declared conventions rank the originally driven family first), and a read-only diagnostic on the archived payload then showed the original selection mechanism was bank-order-first—identical to the orchestrators—refuting the hypothesis and strengthening the epoch findings.

9.2 Candidate filter underived. No predicate over certified-scope component properties reproduces the archived component membership (best near-miss: carrier edges ≥ 10, off by 33 of 421 candidates). This is an open reconstruction gap; it blocks certified scans off the archived state, motivated the archived-scope design of §4, and bounds the epoch counts of §8.

9.3 Quarantined run. One full profiling run executed with unfiltered discovery scans produced phantom high-capacity families and was discarded upon in-context certification failure; its detection mechanism (self-certification against the archived state) is part of the released scaffold.

9.4 Scope limitations. All scored predictions derive from a single substrate (the archived lineage state) and one primary drive per tier; the epoch analysis is single-seed; the debris χ population carries no $\chi = 2$ structure on the certified anchor and was therefore not used for the mapping.

10 Conclusion: A Pre-Registered Challenge to the Continuum

The structural predictions presented here—a softening boundary, a pre-boundary pile-up, and an inversion of the post-boundary deficit at higher energies—are cryptographically locked in advance of the CMS Run-3 dijet angular distribution publications. By pre-registering these directional, falsifiable signatures, we remove the persistent hazard of post-hoc curve fitting that often plagues novel theoretical frameworks.

11 Scoring Plan

Scoring follows frozen §7 against the first relevant Run-3 collaboration publication or HEPData record: directional hits on signs of S^* and Δ^* per bin; magnitude classes scored separately; unweighted Stouffer Z across bins with permutation-based specificity against non-boundary χ bins; bin edges conformed by aggregation only, else VOID. Falsifiers as frozen. Results will be published regardless of outcome [11].

12 Data and Code Availability

Scaffold, frozen packet, ladder records, prediction card, and checksum manifests: `https://github.com/jrmerwin/deu-run3`, tags `run3-protocol-v1` and `run3-values-v1`. Locked predictions, checksums, and ladder records: Zenodo 10.5281/zenodo.21464119. State pickles and oversize enumeration tables: 10.5281/zenodo.21464816. Stage-1 protocol DOI as recorded in the frozen packet, hash-locked via `STATE_SHA256SUMS`. Every scored number is re-derivable from the deposited state and the tagged code.

Acknowledgments

The author acknowledges assistance from Anthropic AI models in code generation and data analysis.

References

[1] CMS Collaboration, "Measurement of dijet angular distributions and search for beyond the standard model physics in proton-proton collisions at $\sqrt{s} = 13$ TeV," arXiv:2603.25458; CMS-EXO-24-011; CERN-EP-2026-057 (2026).

[2] J. Merwin, *Empirical Signatures of a Discrete Topological Vacuum: Correlating LHCb Angular Tensions and CMS Dijet Fractures*, ai.viXra.org:2605.0007 (2026).

[3] J. Merwin, *A Finite Carrier Vacuum and Discrete Collision Fractures in the Distinction Engine*, ai.viXra.org:2606.0063 (2026).

[4] J. Merwin, *Computational Bandwidth Limits Unify Gravitational and Quantum Dynamics in a Discrete Spacetime*,ai.viXra.org:2607.0021 (2026).

[5] J. Merwin, *The Distinction Engine: Recovery of the 137-Element Relational Registry from a Single Logical Axiom*, ai.viXra.org:2604.0057 (2026).

[6] J. Merwin, *The 41/40 Graph Index in the Distinction Engine Universe: Discrete-Substrate Resonance, CMB Amplitude Closure, and Cross-Observable Clock Projections*, ai.viXra.org:2605.0023 (2026).

[7] H. Hoppe et al., *Mesh optimization*, SIGGRAPH (1993).

[8] R. L. Workman et al. (Particle Data Group), *Review of Particle Physics: Searches for Quark and Lepton Compositeness*, Prog. Theor. Exp. Phys. 2022, 083C01 (2022).

[9] E. Eichten, K. Lane, and M. Peskin, *New Tests for Quark and Lepton Substructure*, Phys. Rev. Lett. 50, 811 (1983).

[10] R. Loll, *Quantum Gravity from Causal Dynamical Triangulations: A Review*, Class. Quantum Grav. 37, 013002 (2019).

[11] E. Maguire, L. Heinrich, and G. Watt, *HEPData: a repository for high energy physics data*, J. Phys.: Conf. Ser. 898, 102006 (2017).